ACS APPLIED POLYMER MATERIALS

pubs.acs.org/acsapm Article

Zwitterionic Porous Conjugated Polymers as a Versatile Platform for Antibiofouling Implantable Bioelectronics

Jinjia Xu, Jian Xu, Haesoo Moon, Herman O. Sintim, and Hyowon Lee*

Cite This: *ACS Appl. Polym. Mater.* 2020, 2, 528−536 Read Online

ACCESS | Metrics & More | Article Recommendations | Supporting Information

ABSTRACT: Here, we describe the design, synthesis, and evaluation of two kinds of multifunctional zwitterionic linear poly(carboxybetaine thiophene) (PCBTh) and porous poly(carboxybetaine thiophene-*co*-9,9′-bifluoreneylidene) (PCBTh-*co*BF) polymers, which can be facilely synthesized using Yamamoto and Suzuki polycondensation, respectively. The integrations of zwitterionic polymer-based biomaterials that consist of conjugated polymer backbones, multifunctional zwitterionic side chains, and distorted units are designed and studied to address a key challenge of conjugated polymers in biomedical applications: biofouling phenomena that eventually lead to the failure and reduced lifetime of bioelectronics in the body. The introduction of a twisting unit into the polymer backbone allows us to tune the porosity, morphology, optical properties, and efficiency of antibiofouling features of resulting polymers. The PCBTh-*co*BF coated surface exhibits good conductivity, stability, hydrophilicity, and antibiofouling properties against protein adsorption, cell growth, and bacteria attachment, which may be useful for chronic in vivo bioelectronics applications by minimizing the foreign body response.

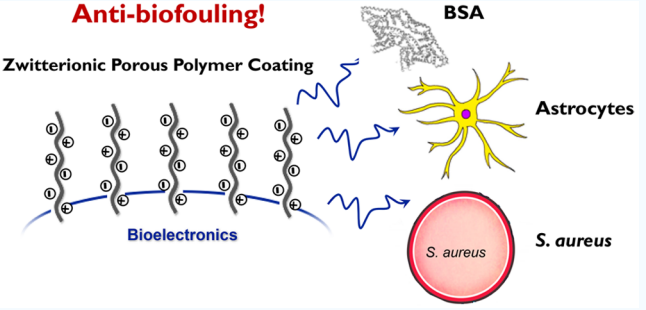

KEYWORDS: *antibiofouling, zwitterionic conjugated polymers, porous conductive polymers, implantable devices, biomaterials*

INTRODUCTION

π-Conjugated polymers (CPs) have attracted considerable amounts of attention for various biomedical applications, including bioelectronics,[1,2] sensing,[3−5] tissue engineering,[6,7] and wound healing,[8] which have benefitted from the structural flexibility, tunable conductivity, flexible mechanical properties, and ease of fabrication of CPs when compared with inorganic conducting materials.[9,10] In previous studies, CPs have been used to improve interfacial interaction between electrochemical devices and biological systems as conducting or sensing biomaterials for more efficient bioelectronic device performance.[11−13] However, biomacromolecules such as proteins, cells, and bacteria tend to adsorb onto hydrophobic CP surfaces that are not originally desirable in complex biological medium. Moreover, it has been shown that the improved electrochemical performance augmented with CPs could not be sustained after in vivo implantation due to the nonspecific adsorption of biomacromolecules on biomedical device surfaces (i.e., biofouling) that reduce the sensitivity and performance of bioelectronic interfaces.[14,15] Biofouling often triggers the foreign body response (FBR) cascade that eventually leads to the failure and reduced lifetime of implantable devices.[16,17] Surface modifications have been extensively explored to increase integration with biological tissues and minimize fibrous encapsulation at complex biointerfaces.[4,5,18] Recently, many researchers focus on biomaterials engineering that involves advanced techniques to alter device interfaces from hydrophobic to hydrophilic using polymer coating techniques.[19] Several research groups have reported that zwitterionic CPs could effectively prevent nonspecific protein adsorption and cell attachments.[20−25] Because there are a large number of relevant applications ranging from the field of solid state technology to biomedical engineering, high-performance CPs that determine the function and properties of devices are of great importance, and the development of novel multifunctional zwitterionic CPs is highly desirable.

In this work, we present the development of porous CPs with antibiofouling properties for improving in vivo performance of bioelectronic devices (Scheme 1). Compared to the conventional CPs established thus far, novel porous organic polymers represent a new type of conductive polymer which exhibits a larger surface area, low mass density, and high stability.[26,27] Porous organic polymers have been widely used in catalysis,[28] gas storage[29,30] and separations,[31−34] drug delivery,[35] sensing, etc.[36] However, the development of

Received: October 7, 2019
Accepted: January 27, 2020
Published: February 5, 2020

https://dx.doi.org/10.1021/acsapm.9b00950
ACS Appl. Polym. Mater. 2020, 2, 528−536

Scheme 1. (A) Design Concept of This Study and (B) Structural Illustration of PCBTh and PCBTh-*co*BF That Consists of the Conjugated Polythiophene Backbone, Tetrasubstituted Zwitterionic Side Chains, and Twisting 9,9′-BF Units for PCBTh-*co*BF[a]

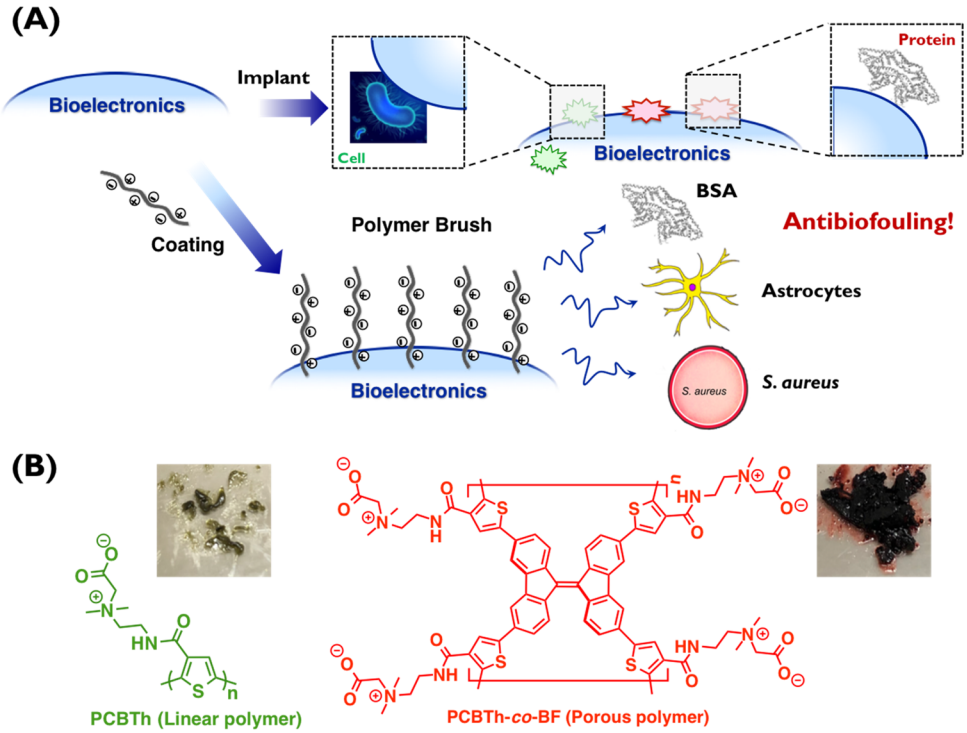

[a]Compared with nonconducting zwitterionic materials, the conjugated backbone helps gain electronic conductivity, and the nonbiocompatible CPs obtain excellent biocompatibility. Moreover, the twisting unit insertion provides enough free volume inside zwitterionic CP networks to construct a porous skeleton, bioconjugation functionality, and superior antibiofouling properties via tetrasubstituted zwitterionic side chains.

zwitterionic CPs with porosity exhibiting excellent antibiofouling properties against multiple biomacromolecules for implantable bioelectronics devices has not yet been reported despite the potential to achieve more advanced functionality in biosensors and bioelectronics. The 9,9′-bifluoreneylidene (9,9′-BF) is a well-known distorted building block, where two fluorene units are connected through a C═C bond with a 30° twisting angle because of the steric hindrance of peripheral 1-H and 8-H.[37,38] We hypothesize that such twisted conformation would provide enough free volume inside zwitterionic CP networks to construct a porous skeleton.

To test our hypothesis, we designed and successfully synthesized thiophene-based conjugated linear (PCBTh) and porous (PCBTh-*co*BF) polymers via Yamamoto and Suzuki polycondensation. The porous PCBTh-*co*BF consists of conjugated polymer backbones, multifunctional zwitterionic side chains, and a distorted 9,9′-BF unit in core components (Scheme 1). Conjugated polythiophene was selected as the conjugated backbone due to its good electrical conductivity, chemical stability, and unique electronic and optical properties.[39] We chose the zwitterionic carboxybetaine as the side chain because of its excellent antibiofouling property, good water solubility, and biocompatibility.[17] Both linear and porous CPs demonstrated effective antibiofouling properties against proteins, cells, and bacteria while maintaining good conductivity. The ultraviolet−visible spectrophotometry showed interesting photophysical properties of both polymers in solution and film states. Using scanning electron microscopy (SEM) and transmission electron microscopy (TEM), we confirmed the porous morphology of PCBTh-*co*BF. We demonstrated that the porosity, optical, and electronic properties of polymers can readily be tuned by insertion of distorted 9,9′-BF units. Based on our evaluations, we expect both PCBTh and PCBTh-*co*BF may be used to serve as multifunctional protective layers to resist protein adsorption, inhibit bacteria growth, and prevent cell attachment, thereby potentially prolonging the lifetime of implanted bioelectronics devices.

RESULTS AND DISCUSSION

Synthesis and Characterization. As depicted in Figure 1, we synthesized two monomers, M1 and M2, in a simple manner using readily available starting materials. The PCBTh was synthesized using monomer M1 through ^{0}Ni-catalyzed Yamamoto coupling reaction.[40] The resulting PCBTh is a sticky light-green solid (Scheme 1B), which exhibited good solubility in common organic solvents and is especially highly soluble in methanol. The monomers M1 and M2 were copolymerized via palladium-catalyzed Suzuki polycondensation to obtain PCBTh-*co*BF, which is a sticky solid with dark red color (Scheme 1). The PCBTh-*co*BF also exhibited good solubility in common organic solvents such as methanol. We verified the chemical structures of PCBTh and PCBTh-*co*BF using NMR and MS spectra (Supporting Information).

It has been demonstrated that the porous nanostructures of CPs are highly favorable for electrochemical sensing and detection.[41] Using SEM and TEM, we verified the morphologies of two polymers, which confirmed the desired porous nanostructure of PCBTh-*co*BF compared to the morphology of PCBTh (Figure 2). This result suggests that

https://dx.doi.org/10.1021/acsapm.9b00950
ACS Appl. Polym. Mater. 2020, 2, 528−536

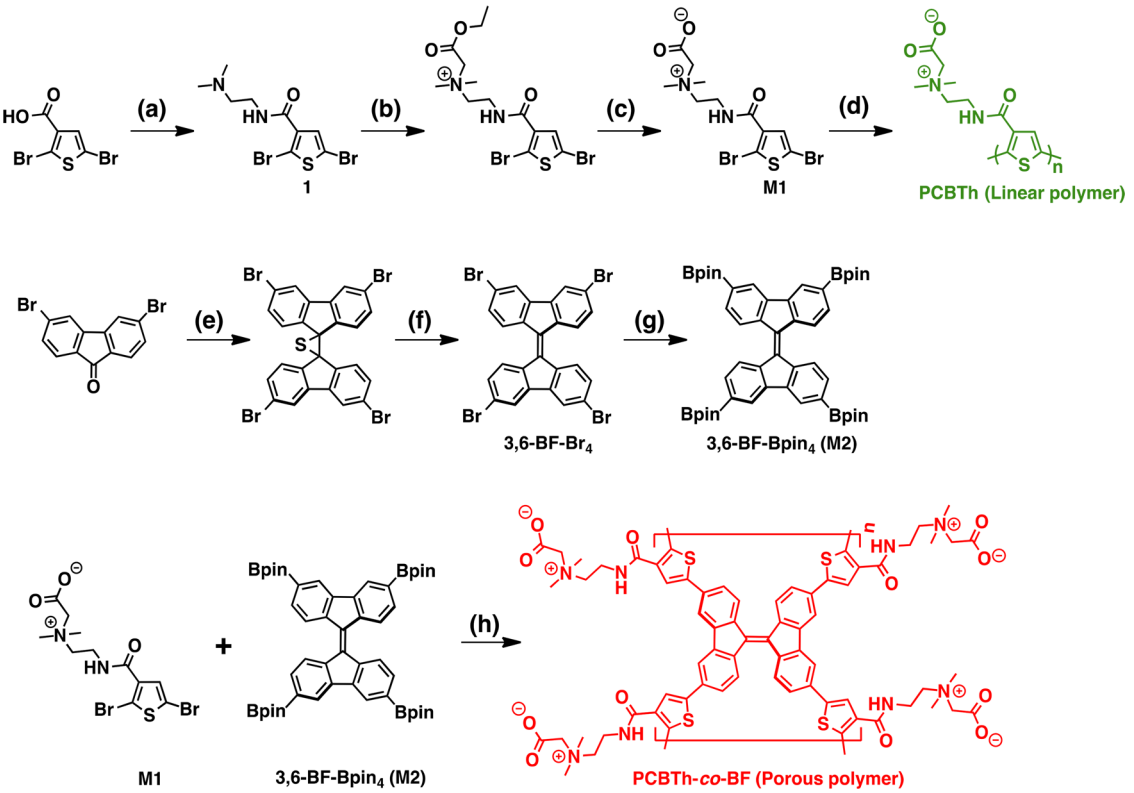

Figure 1. Synthetic routes to obtain PCBTh and PCBTh-*co*BF. Reagents and conditions: (a) 1,1′-carbonyldiimidazole (CDI), *N*,*N*′-dimethylethylenediamine, THF, 0 °C, 24 h; (b) ethyl bromoacetate, 60 °C, 2 days; (c) NaOH, H_2O; (d) $Ni(COD)_2$, 2,2′-bipyridyl, COD, DMF, and toluene, 90 °C, 48 h; (e) Lawesson's reagent, toluene, reflux, overnight; (f) copper power, toluene, reflux, 3 h; (g) $(Bpin)_2$, KOAc, $Pd(dppf)Cl_2$, 1,4-dioxane, 110 °C, 72 h; (h) $Pd(PPh_3)_4$, Na_2CO_3, toluene, H_2O, EtOH, reflux, overnight.

the insertion of the 9,9′-BF twisted unit into the conjugated polymer backbone is an efficient strategy to tune the morphology of resultant polymers and provides alternative methods to create nano- or mesoporous CPs. We also evaluated the thermal properties of two polymers using differential scanning calorimetry (DSC) measurements. As shown in Figure S1, both PCBTh-*co*BF and PCBTh showed relatively low glass transition temperatures, which were found at 30 and 36 °C, respectively.

Next, we systematically investigated the photophysical and electrochemical properties of PCBTh and PCBTh-*co*BF. The UV−vis absorption of PCBTh in methanol solution at 298 K is shown in Figure 3A, exhibiting intense absorption in the visible range with an absorption maximum at 307 nm (green solid line). Following the insertion of the 9,9′-BF twisted unit, an intense absorption peak is additionally observed for PCBTh-*co*BF with an absorption maximum at 491 nm (red solid line), which originates from the M2 building block (Figure 3B). These results also indicated that the M1 and M2 were covalently connected to each other in the PCBTh-*co*BF backbone. The absorption spectra of PCBTh-*co*BF in the thin-film state (red dashed line) are 18 nm red-shifted relative to the result from methanol solution spectra with a maximum absorption band at 333 nm, while the absorption band from the twisted 9,9′-BF unit at 491 nm did not exhibit any peak shifts. We determined that the optical bandgaps (E_g) of PCBTh-*co*BF estimated from the onset of absorption to be 1.86 eV (Figure 3) versus 3.59 eV from PCBTh. The comparable absorption spectra and optical bandgaps between PCBTh and PCBTh-*co*BF suggest that the introduction of the twisted 9,9′-BF unit has a significant effect on the photophysical properties of resultant polymers. The fluorescent emissions from PCBTh-*co*BF and PCBTh were negligible in solution and film states (Figure S2). It should be noted that it is important to minimize the background fluorescence of the biomaterial to support experiments using fluorescent biological matrices in evaluation of each material's antibiofouling properties.[42]

The electrochemical processes in complex biological systems generally require efficient transportation of ions and electrons. We envisioned the zwitterionic conjugated PCBTh and PCBTh-*co*BF polymers to have electron conductivity via conjugated polymer backbones. Cyclic voltammetry (CV) measurements were used to investigate electrochemical properties of thin-film PCBTh and PCBTh-*co*BF polymers (Figure S3). The PCBTh and PCBTh-*co*BF showed comparable overall electrical conductivity relative to that of previously reported zwitterionic polymers.[43] Electrical conductivity was calculated to be 8.1×10^{-5} and 6.7×10^{-5} mS·cm^{-1}, respectively.

The hydrophilicity of PCBTh and PCBTh-*co*BF coated surfaces is an important feature in an implantable substrate. Thus, we quantified the wettability of the polymer-coated surfaces by measuring the contact angle of a water droplet deposited onto the glass surface. As shown in Figure 4, the water contact angle on a pristine glass substrate was measured to be 70.9°, while the contact angles on PCBTh and PCBTh-*co*BF coated surfaces were 22.6° and 36.5°, respectively. This result suggests an increase in hydrophilicity from both polymer-coated surfaces. It should be noted that the PCBTh coated surface showed a smaller contact angle with more hydrophilicity than that of the PCBTh-*co*BF treatment,

https://dx.doi.org/10.1021/acsapm.9b00950
ACS Appl. Polym. Mater. 2020, 2, 528−536

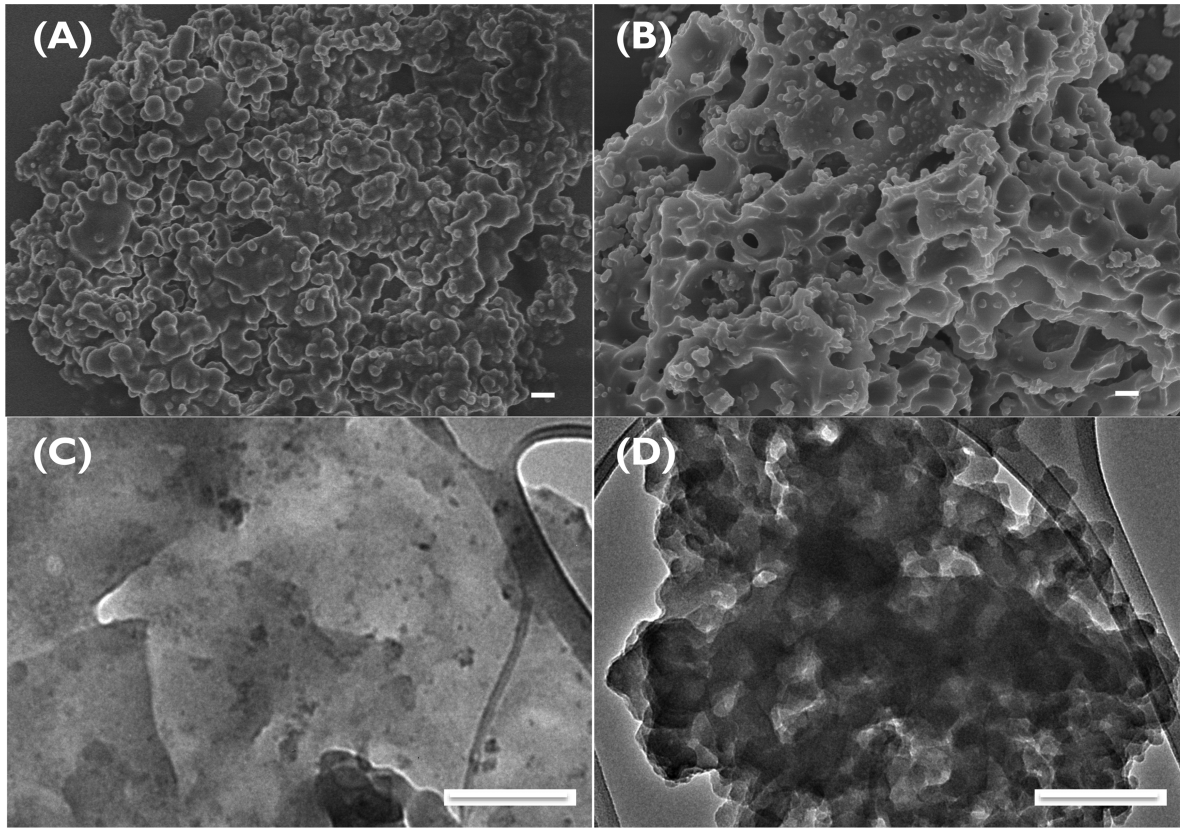

Figure 2. SEM images of (A) PCBTh linear polymer and (B) PCBTh-*co*BF porous polymer (scale bar: 500 nm) and TEM images of (C) PCBTh linear polymer and (D) PCBTh-*co*BF porous polymer (scale bar: 250 nm).

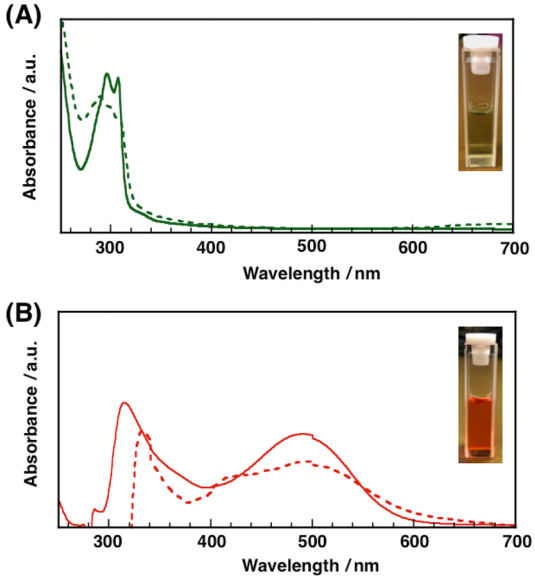

Figure 3. UV−vis absorption spectra of (A) PCBTh and (B) PCBTh-*co*BF dissolved in methanol solution (solid lines) and in thin-film state as deposited (dashed lines) at room temperature. Inset: photos of polymers dissolved in methanol solution.

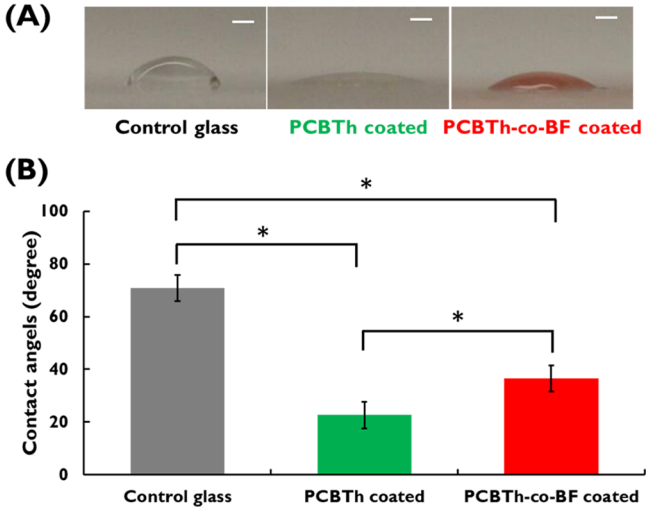

Figure 4. (A) Pictures of water droplets deposited on tested surfaces and (B) contact angle (degrees) comparison for control noncoating (control glass), PCBTh coated, and PCBTh-*co*BF coated glass surfaces (scale bar: 1 mm). A significant decrease in contact angle was visualized for the PCBTh coated surface compared to that of the PCBTh-*co*BF coated surface, which is probably because of a more effective and condensed coating. Data represent mean ± SD (n = 3), *p < 0.001, calculated using one-way ANOVA (analysis of variance) with Bonferroni test.

probably due to the large steric hindrance from the 9,9′-BF twisted unit that may limit surface coverage.

The FBR begins by initiating a cascade of physicochemical reactions which are triggered by nonspecifically adsorbed biomacromolecules, eventually leading to the formation of a fibrous capsule.[44] Thus, we are interested in minimizing the amount of adsorbed protein to prevent the initiation of an inflammatory cascade. Our original hypothesis is that the FBR may be reduced if the implanted surface can effectively prevent nonspecific biomolecular adsorptions. Thus, we wanted to

https://dx.doi.org/10.1021/acsapm.9b00950
ACS Appl. Polym. Mater. 2020, 2, 528−536

evaluate whether the zwitterionic side chain attachments will endow PCBTh and PCBTh-*co*BF with superior antibiofouling properties to resist protein adsorption, cell attachment, and bacteria growth on their surfaces. Such super antibiofouling materials and surfaces are highly desired for various biomedical applications.

Protein-Based Biofouling Adhesion. First, we tested the protein adsorption on polymer coated glass substrates. The commonly used protein, bovine serum albumin (BSA), was utilized to demonstrate the antiprotein property of PCBTh and PCBTh-*co*BF coated surfaces. To maximize the fluorescence intensity, we incubated pristine glass substrates in varying concentrations of fluorescein-conjugated BSA (BSA-FITC) solution (2−10 mg/mL) in phosphate buffered solution (PBS, n = 3, each) for 2 h. As shown in Figure S4, the fluorescence intensity of absorbed BSA-FITC gradually increased and became saturated at a concentration of 6 mg/mL in PBS.

To examine antibiofouling capability against BSA-FITC attachment, we incubated various test samples with different polymer coatings in BSA-FITC solution (6 mg/mL) for 2 h to evaluate the amount of adsorbed protein on pristine versus polymer-coated glass substrates (Figure 5A). Using a fluorescence microscope, we captured images of each sample and quantified the fluorescence intensity using ImageJ.[45] Figures 5A−C compare the fluorescence between each sample and shows clear differences in fluorescence intensity. The results show that the fluorescence intensity of PCBTh coated surface was significantly reduced up to 84% compared to the pristine glass substrate. When coated with PCBTh-*co*BF, we can see an even greater BSA-FITC reduction of 94%. Figure 5D and Table 1 highlight the differences in fluorescence intensity between pristine glass substrate, PCBTh, and PCBTh-*co*BF coated surfaces. It should be noted that reproducibility of these results was examined and shown to be consistent in Figures S5 and S6.

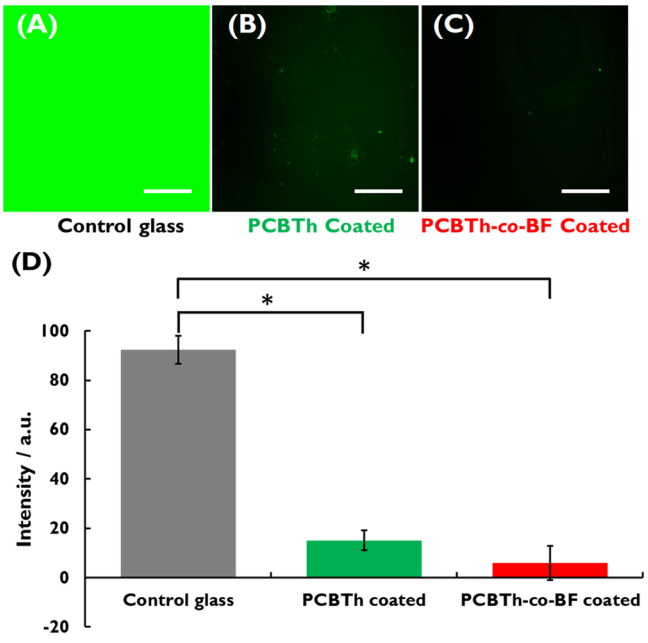

Figure 5. Fluorescence images of (A) BSA-FITC on pristine glass surface, (B) BSA-FITC on PCBTh-coated glass surface, and (C) BSA-FITC on PCBTh-*co*BF-coated glass surface (scale bar: 200 μm). (D) Comparison of fluorescence intensity. n = 3 for each sample, *p < 0.001, calculated using one-way ANOVA with Bonferroni test.

Table 1. Percentage of the Protein Adhesion and the Coverage of Cells Attachment on Pristine and Polymer-Coated Glass Surfaces (n = 3)

	control glass	PCBTh coated	PCBTh-*co*BF coated
% of BSA adhesion	92.3 ± 5.6	15.1 ± 4.1	5.9 ± 4.3
% of astrocytes coverage	23.58 ± 1.59	0.54 ± 0.23	0.004 ± 0.004

Cell Attachment Study. Astrocytes are important immunological components of the central nervous system, participating in synaptic plasticity and information processing in the neuronal circuit. They exert metabolic effects, provide structural support for neurons, and play a role in modulating neuron homeostasis and higher neuronal functions. The interaction between astrocytes and neurons plays a crucial role in the development and progression of diverse neurological disorders.[46] To further evaluate the antibiofouling properties of the PCBTh and PCBTh-*co*BF coated surfaces, we performed cell attachment studies using astrocytes. These cultures were incubated to reach the confluency (48 h) in a humidified atmosphere with 5% CO_2 at 37 °C. The cell culture medium was replaced 1 day after seeding. As it can be seen in Figure 6A, a large amount of astrocyte cells readily attached to the uncoated glass substrate (with coverage of 23.58%), while very few cells were found on the PCBTh coated glass substrate, and almost no cells were visible on the PCBTh-*co*BF coated glass substrate (Figures 6B and 6C). The coverage of astrocyte cells on PCBTh and PCBTh-*co*BF coated surfaces was

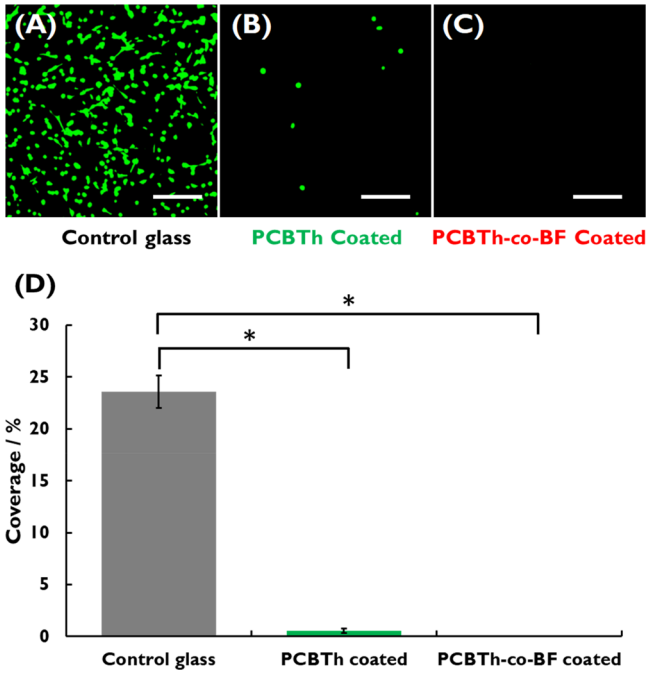

Figure 6. Representative fluorescence microscopy images of astrocyte cells attached on (A) pristine glass substrate, (B) PCBTh-coated glass surface, and (C) PCBTh-*co*BF-coated glass surface after 48 h incubation in PBS buffer solution (scale bar: 200 μm). (D) Percent cell coverage on the surfaces with different treatments. n = 3 for each sample, *p < 0.001, calculated using one-way ANOVA with Bonferroni test.

https://dx.doi.org/10.1021/acsapm.9b00950
ACS Appl. Polym. Mater. 2020, 2, 528−536

evaluated to be 0.54 and 0.004%, respectively (Figure 6D and Table 1). These results support our hypothesis that polymer coated surfaces can effectively resist adherent cell attachments as well. It should be noted that reproducibility of these results is examined and consistently shown in Figures S7 and S8.

Biofilm in Vitro Arrays. A major issue for implantable devices is the risk of infection. The ability for *Staphylococcus aureus* (*S. aureus*) bacteria to adhere and proliferate on implantable biomedical devices is regarded as one of the major challenges in the biomedical field. *S. aureus* biofilms are able to tolerate high doses of antibiotics, and the ability to initiate infection on implantable devices is a serious ongoing challenge.[47] Infections may be avoided by inhibiting initial adhesion of bacteria to the substrate surface, thus eliminating the possibility for an infection to occur on the surface of implants and diffuse to the surrounding areas. Thus, we investigated the antimicrobial properties of PCBTh and PCBTh-*co*BF. Various glass samples with and without polymer coatings were incubated in *S. aureus* culture solution at 37 °C for 48 h to quantify the amount of adherent bacteria coverage. We wanted to evaluate whether these polymer coating surfaces had the potential to inhibit *S. aureus* adhesion and growth. Using confocal laser scanning microscopy, we quantified the amount of live (green) and dead (red) bacteria on various glass samples following the incubation period. Afterward, the coverage of bacteria cells was evaluated.

As shown in Figures 7B and 7C, our results suggest that the glass substrate coated with PCBTh can inhibit *S. aureus* attachment during the 48 h incubation. Similarly, the PCBTh-*co*BF coated surface exhibited a significant reduction in bacterial growth compared to the noncoated control glass substrate (Figures 7A–C). The amount of *S. aureus* on each surface is summarized in Figure 7D and Table 2. To provide a proof-of-concept, in vitro experiments indicate that the PCBTh and PCBTh-*co*BF coatings on implantable material surfaces can provide a promising platform to resist adherence and colonization of biofilm-forming bacteria. We suspect the antibiofouling properties of PCBTh and PCBTh-*co*BF coated surfaces are due to their robust hydration features.

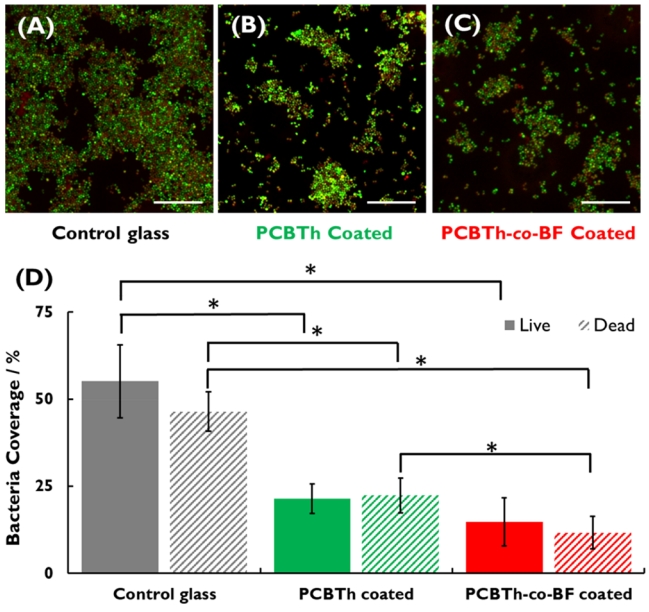

Figure 7. Representative CLSM images of *S. aureus* incubated on (A) pristine glass substrate, (B) PCBTh-coated glass surface, and (C) PCBTh-*co*BF-coated glass surface for 48 h (scale bar: 20 μm). (D) Quantitative percentages of bacteria coverage on these surfaces. $n = 3$ for each sample, $^*p < 0.001$, calculated using two-way ANOVA with Bonferroni test.

CONCLUSIONS

In summary, we designed and synthesized two kinds of zwitterionic CPs which integrate multiple functions into one material. The introduction of a twisting unit into conjugated polymer backbone allows us to tune the porosity, morphology, optical properties, and efficiency of antibiofouling features of resulting polymers. Polymer-coated surfaces were extensively characterized by means of SEM and TEM visualization, contact angle measurement, and fluorescent microscopy. These new biomaterials showed significant antibiofouling properties with a great resistance to protein adsorption, cell attachment, and bacteria growth. The results presented here also provided a better understanding of structure–property–function relationships among zwitterionic conjugated polymers. This versatile platform can potentially be adapted to a wide range of applications for bioelectronics, organic electrochemical transistors, and biofuel cells, which require high-performance conducting materials with excellent antibiofouling properties.

EXPERIMENTAL SECTION

Materials. 1,1′-Carbonyldiimidazole (CDI), 2,5-dibromothiophene-3-carboxylic acid, *N*-hydroxysuccinimide (NHS), and tris(2-carboxyethyl)phosphine hydrochloride (TCEP) were purchased from Chem-Impex International (Wood Dale, IL, United States). Thermo initiator 2,2′- azobis[2-(2-imidazolin-2-yl)propane]dihydrochloride (VA-044) was purchased from Wako Chemicals USA, Inc. (Richmond, VA, United States). Anhydrous tetrahydrofuran (THF), anhydrous chloroform, methanol, dichloromethane, ethyl acetate, acetonitrile, cystaminedihydrochloride, *N*,*N*′-dimethylethylenediamine, ethyl bromoacetate, anhydrous $FeCl_3$, sodium hydroxide, and glucose were purchased from Sigma-Aldrich (St. Louis, MO, United States). All chemicals were used as received without further purification. Milli-Q water (18.2 MW/cm, Burlington, MA) was used. Air and water sensitive synthetic manipulations were performed under an N_2 atmosphere using standard Schlenk techniques. Human cerebral cortex astrocytes, astrocyte medium, cell freezing medium, fetal bovine serum, astrocyte growth supplement, and penicillin/streptomycin solution were purchased from ScienCell Researh Laboratories (Carlsbad, CA). CellTracker green CMFDA dye, phosphate-buffered saline (PBS, 10×, pH 7.4), albumin from bovine serum fluorescein conjugate (FITC-BSA), Dulbecco's phosphate-buffered saline (no calcium, no magnesium) (DPBS), poly-D-lysine, and LIVE/DEAD BacLight Bacterial Viability Kit were purchased from ThermoFisher Scientific (Waltham, MA). Tryptic soy broth (TSB) was purchased from Becton Dickinson (Franklin Lakes, NJ). Diced microscope slides and cover glass from Fisher Scientific

Table 2. Percentages of the *S. aureus* Coverage on Pristine and Polymer-Coated Surfaces ($n = 3$)

control glass		PCBTh coated		PCBTh-*co*BF coated	
live *S. aureus* (%)	dead *S. aureus* (%)	live *S. aureus* (%)	dead *S. aureus* (%)	live *S. aureus* (%)	dead *S. aureus* (%)
55.15 ± 10.46	46.41 ± 5.69	21.40 ± 4.23	22.34 ± 4.95	14.75 ± 6.86	11.69 ± 4.73

https://dx.doi.org/10.1021/acsapm.9b00950
ACS Appl. Polym. Mater. 2020, 2, 528–536

(Pittsburgh, PA) were used as glass substrate after cleaning and drying.

Instruments. NMR spectra were recorded on a JEOL ECS-500 (500 MHz) spectrometer by using tetramethylsilane (0 ppm for ^{1}H NMR) as an internal standard. MALDI/TOF-MS measurements were performed on an AXIMA−CFR Plus (Shimadzu) with dithranol as a matrix. The UV−vis absorption spectra were recorded on a JASCO V-670 spectrophotometer in a quartz cuvettes of 1 mm path length. The PerkinElmer LS 55 fluorescence spectrometer (Waltham, MA, United States) was used to collect the fluorescence emission spectra of polymers. The surface morphology was captured using Hitachi S-4800 Field Emission SEM scanning electron microscope with 5 kV as accelerating voltage and analyzed using ImageJ. For TEM imaging, samples were prepared by pipetting isopropyl alcohol (IPA) solutions of PCBTh and PCBTh-*co*BF on a lacey carbon TEM grids. TEM images were captured using a Tecnai G2 20 transmission electron microscope at 200 kV. The biofilms were examined using a ZEISS LSM 880 confocal laser scanning microscope (CLSM). Z-stack images at 100× magnification were taken and analyzed using Zeiss Zen software and MATLAB.

Polymer Thin-Film Preparation. Thin-films of polymer were fabricated with a graft-to method. The polymers were dissolved in methanol at a concentration of 10 mg/mL. One-hundred microliters of polymer methanol solution was deposited on a glass substrate. It was first put in a Petri dish and left undisturbed until solvent evaporated at room temperature. The samples were washed with PBS buffer solution and dried with filtered air prior to characterization.

Contact Angle Measurements. Contact angle measurements were conducted by analyzing the photographic pictures of water droplets applied on respective samples. A 5 μL droplet of DI water was applied to on the surface of 1 cm^2 chips of untreated, PCBTh coated, or PCBTh-*co*BF coated glass substrate surfaces, and the contact angles of the static droplets were evaluated between the solid−liquid and liquid−air interfaces. Measurements were performed in triplicate.

Electrochemical Characterization of Polymers. Electrochemical analysis of polymers was performed using a SP-200 potentiostat (Biologic USA, LLC, Knoxville, TN, United States). PCBTh and PCBTh-*co*BF thin-films were coated on the surface of the working electrode. All electrochemical experiments were performed in a conventional three electrode cell configuration in 1× PBS (pH 7.0) as the supporting electrolyte (50 mL for all experiments). A scan rate of 100 mV/s and sampling interval of 1 mV/s were used for cyclic voltammetry (CV).

BSA-FITC Culture. We tested the antibiofouling performance of polymer-coated surfaces against protein by comparing fluorescence intensity of respective samples incubated with BSA-FITC. Untreated, PCBTh coated, or PCBTh-*co*BF coated cover glasses were incubated with BSA-FITC in 1X PBS solution of various concentrations in 6-well plates for 2 h. After that, samples were gently rinsed with 1X PBS solution before imaging using a fluorescence microscope (Axio Observer Z1, Carl Zeiss Microscopy, Jena, Germany) with a filter set 17 (excitation, BP 485/20, and emission BP 515−565, Carl Zeiss Microscopy, LLC). Image intensities were quantified using ImageJ.

Cell Culture, Staining, and Reagents. Astrocyte medium contained 500 mL of basal medium, 10 mL of fetal bovine serum (FBS, Cat. No. 0010), 5 mL of astrocyte growth supplement (AGS, Cat. No. 1852), and 5 mL of penicillin/streptomycin solution (P/S, Cat. No. 0503). Human cerebral cortex astrocytes were cryopreserved at passage one. Astrocytes were expanded and maintained per Sciencell's protocol. Astrocytes were cultured in 12-well, tissue culture-treated plates, with 1 × 10^5 cells seeded per well. These cultures were then incubated until confluent (48 h) in a humidified atmosphere with 5% CO_2 at 37 °C. The medium was replaced 1 day after seeding. Cells were stained with CellTracker Green CMFDA. We replaced cell culture medium in each well with a 1:1000 ratio of dye to medium and incubated at 37 °C for 30 min.

***S. Aureus* in Vitro Adherence Assay, Strain, and Reagents.** We tested the antibiofouling performance of polymer-coated surfaces against bacteria by comparing the coverage of live and dead bacteria on respective samples incubated with *Staphylococcus aureus* (*S. aureus*). Erythromycin-resistant *S. aureus* tagged with green fluorescent protein (GFP) were used. Prior to each experiment, bacteria cultures were refreshed from stocks in 19:1:0.02 (v:v:v) TSB: 20% (w/v) glucose: erythromycin medium at 37 °C for 12 h at 250 rpm. After that, bacteria cultures were diluted to 1/1000 into the same growth medium. To start the biofilm growth, 5 mL of the bacteria solution was then aliquoted to each sample, which was previously incubated in 5 mL of 1:9 (v:v) poly-D-lysine: 1× PBS solution for 12 h at room temperature to facilitate bacteria attachment. After incubation at 37 °C for 48 h at 50 rpm, 1.5 μL propidium iodide (PI) from bacterial viability kit was added to stain the dead bacteria. After the aspiration of bacteria solution and proper air drying, the biofilms were examined using a confocal laser scanning microscope (ZEISS LSM 880, Carl Zeiss, Jena, Germany)). Images at 100× magnification were taken and analyzed using Zeiss Zen software.

■ ASSOCIATED CONTENT

Supporting Information

The Supporting Information is available free of charge at https://pubs.acs.org/doi/10.1021/acsapm.9b00950.

Synthetic procedures of monomers and polymers, NMR data, DSC, fluorescence spectra, cyclic voltammograms of both polymers, and fluorescence microscope images of polymer coated surfaces when incubated with BSA-FITC and astrocytes (PDF)

■ AUTHOR INFORMATION

Corresponding Author

Hyowon Lee − *Weldon School of Biomedical Engineering, Birck Nanotechnology Center, Center for Implantable Devices, Purdue University, West Lafayette, Indiana 47906, United States;* orcid.org/0000-0001-7628-1441; Email: hwlee@purdue.edu

Authors

Jinjia Xu − *Weldon School of Biomedical Engineering, Birck Nanotechnology Center, Center for Implantable Devices, Purdue University, West Lafayette, Indiana 47906, United States*

Jian Xu − *Weldon School of Biomedical Engineering, Birck Nanotechnology Center, Center for Implantable Devices, Purdue University, West Lafayette, Indiana 47906, United States*

Haesoo Moon − *Weldon School of Biomedical Engineering, Birck Nanotechnology Center, Center for Implantable Devices, Purdue University, West Lafayette, Indiana 47906, United States*

Herman O. Sintim − *Department of Chemistry, Center for Drug Discovery, Purdue Institute of Inflammation, Immunology and Infectious Disease, Purdue University, West Lafayette, Indiana 47906, United States*

Complete contact information is available at: https://pubs.acs.org/10.1021/acsapm.9b00950

Notes

The authors declare no competing financial interest.

■ ACKNOWLEDGMENTS

This work was supported in part by the National Science Foundation (United States) under Grants ECCS-1944480 and CNS-1726865, the Global Research Outreach program of Samsung Advanced Institute of Technology, and Eli Lilly Connected Care Program. The authors are grateful to Dr. Bryan Boudouris for allowing access to his laboratory during the polymer synthesis. The authors would also like to thank

Mr. Jim Nolan for his assistance with cell culture experiments, Dr. Christopher J Gilpin and Shoumya Nandy Shuvo for their help with TEM characterization, and Dr. Youlong Zhu for his assistance with conductivity measurements of polymers.

REFERENCES

(1) Lanzani, G. Materials for Bioelectronics: Organic Electronics Meets Biology. *Nat. Mater.* **2014**, *13*, 775−776.
(2) Molino, P. J.; Wallace, G. G. Next Generation Bioelectronics: Advances in Fabrication Coupled with Clever Chemistries Enable the Effective Integration of Biomaterials and Organic Conductors. *APL Mater.* **2015**, *3*, 014913−014925.
(3) Green, R. A.; Lovell, N. H.; Poole-Warren, L. A. Cell Attachment Functionality of Bioactive Conducting Polymers for Neural Interfaces. *Biomaterials* **2009**, *30*, 3637−3644.
(4) Abidian, M. R.; Martin, D. C. Multifunctional Nanobiomaterials for Neural Interfaces. *Adv. Funct. Mater.* **2009**, *19*, 573−585.
(5) Abidian, M. R.; Martin, D. C. Experimental and Theoretical Characterization of Implantable Neural Microelectrodes Modified with Conducting Polymer Nanotubes. *Biomaterials* **2008**, *29*, 1273−1283.
(6) Schmidt, C. E.; Shastri, V. R.; Vacanti, J. P.; Langer, R. Stimulation of Neurite Outgrowth Using an Electrically Conducting Polymer. *Proc. Natl. Acad. Sci. U. S. A.* **1997**, *94*, 8948−8953.
(7) Garner, B.; Georgevich, A.; Hodgson, A. J.; Liu, L.; Wallace, G. G. Polypyrrole-Heparin Composites as Stimulus-Responsive Substrates for Endothelial Cell Growth. *J. Biomed. Mater. Res.* **1999**, *44*, 121−129.
(8) Collier, J. H.; Camp, J. P.; Hudson, T. W.; Schmidt, C. E. Synthesis and Characterization of Polypyrrole−Hyaluronic Acid Composite Biomaterials for Tissue Engineering Applications. *J. Biomed. Mater. Res.* **2000**, *50*, 574−584.
(9) McQuade, D. T.; Pullen, A. E.; Swager, T. M. Conjugated Polymer-Based Chemical Sensors. *Chem. Rev.* **2000**, *100*, 2537−2574.
(10) Heeger, A. J. Semiconducting and Metallic Polymers: The Fourth Generation of Polymeric Materials. *Angew. Chem., Int. Ed.* **2001**, *40*, 2591−2611.
(11) Green, R. A.; Lovell, N. H.; Wallace, G. G.; Poole-Warren, L. A. Conducting Polymers for Neural Interfaces: Challenges in Developing an Effective Long-Term Implant. *Biomaterials* **2008**, *29*, 3393−3399.
(12) Cui, X. Y.; Martin, D. C. Fuzzy Gold Electrodes for Lowering Impedance and Improving Adhesion with Electrodeposited Conducting Polymer Films. *Sens. Actuators, A* **2003**, *103*, 384−394.
(13) Green, R. A.; Baek, S.; Poole-Warren, L. A.; Martens, P. J. Conducting Polymer-Hydrogels for Medical Electrode Applications. *Sci. Technol. Adv. Mater.* **2010**, *11*, 014107−014120.
(14) Gerritsen, M.; Kros, A.; Sprakel, V.; Lutterman, J. A.; Nolte, R. J. M.; Jansen, J. A. Biomaterial Developments for Bone Tissue Engineering. *Biomaterials* **2000**, *21*, 71−78.
(15) Ratner, B. D. *Biomaterials Science: An Introduction to Materials in Medicine*, 2nd ed.; Elsevier Academic Press: Amsterdam, Boston, 2004.
(16) Green, R. A.; Lovell, N. H.; Poole-Warren, L. A. Cell Attachment Functionality of Bioactive Conducting Polymers for Neural Interfaces. *Biomaterials* **2009**, *30*, 3637−3644.
(17) Zhang, L.; Cao, Z.; Bai, T.; Carr, L.; Menye, J.-R.-E.; Irvin, C.; Ratner, B. D.; Jiang, S. Zwitterionic Hydrogels Implanted in Mice Resist the Foreign-Body Reaction. *Nat. Biotechnol.* **2013**, *31*, 553−556.
(18) Lin, X.; Jain, P.; Wu, K.; Hong, D.; Hung, H.-C.; O'Kelly, M. B.; Li, B.; Zhang, P.; Yuan, Z.; Jiang, S. Ultralow Fouling and Functionalizable Surface Chemistry Based on Zwitterionic Carboxybetaine Random Copolymers. *Langmuir* **2019**, *35*, 1544−1551.
(19) Ngo, B. K. D.; Grunlan, M. A. Protein Resistant Polymeric Biomaterials. *ACS Macro Lett.* **2017**, *6*, 992−1000.
(20) Cao, B.; Tang, Q.; Li, L. L.; Lee, C. J.; Wang, H.; Zhang, Y. Q.; Castaneda, H.; Cheng, G. Integrated Zwitterionic Conjugated Poly(Carboxybetaine Thiophene) as a New Biomaterial Platform. *Chem. Sci.* **2015**, *6*, 782−788.
(21) Cao, B.; Lee, C.-J.; Zeng, Z.; Cheng, F.; Xu, F.; Cong, H.; Cheng, G. Electroactive Poly(Sulfobetaine-3,4-Ethylenedioxythiophene) (PSBEDOT) with Controllable Antifouling and Antimicrobial Properties. *Chem. Sci.* **2016**, *7*, 1976−1981.
(22) Pan, L. J.; Yu, G. H.; Zhai, D. Y.; Lee, H. R.; Zhao, W. T.; Liu, N.; Wang, H. L.; Tee, B. C. K.; Shi, Y.; Cui, Y.; Bao, Z. N. Hierarchical Nanostructured Conducting Polymer Hydrogel with High Electrochemical Activity. *Proc. Natl. Acad. Sci. U. S. A.* **2012**, *109*, 9287−9292.
(23) Cao, B.; Li, L. L.; Tang, Q.; Cheng, G. The Impact of Structure on Elasticity, Switchability, Stability and Functionality of an All-in-One Carboxybetaine Elastomer. *Biomaterials* **2013**, *34*, 7592−7600.
(24) Cao, B.; Li, L.; Wu, H.; Tang, Q.; Sun, B.; Dong, H.; Zhe, J.; Cheng, G. Zwitteration of Dextran: a Facile Route to Integrate Antifouling, Switchability and Optical Transparency into Natural Polymer. *Chem. Commun.* **2014**, *50*, 3234−3237.
(25) Cao, B.; Tang, Q.; Li, L. L.; Humble, J.; Wu, H.; Liu, L.; Cheng, G. Switchable Antimicrobial and Antifouling Hydrogels with Enhanced Mechanical Properties. *Adv. Healthcare Mater.* **2013**, *2*, 1096−1102.
(26) Das, S.; Heasman, P.; Ben, T.; Qiu, S. Porous Organic Materials: Strategic Design and Structure−Function Correlation. *Chem. Rev.* **2017**, *117*, 1515−1563.
(27) McKeown, N. B.; Makhseed, S.; Budd, P. M. Phthalocyanine-Based Nanoporous Network Polymers. *Chem. Commun.* **2002**, 2780−2781.
(28) Li, B.; Guan, Z.; Wang, W.; Yang, X.; Hu, J.; Tan, B.; Li, T. Highly Dispersed pd Catalyst Locked in Knitting Aryl Network Polymers for Suzuki-Miyaura Coupling Reactions of Aryl Chlorides in Aqueous Media. *Adv. Mater.* **2012**, *24*, 3390−3395.
(29) Chen, Q.; Luo, M.; Hammershoj, P.; Zhou, D.; Han, Y.; Laursen, B. W.; Yan, C.; Han, B. H. Microporous Polycarbazole with High Specific Surface Area for Gas Storage and Separation. *J. Am. Chem. Soc.* **2012**, *134*, 6084−6087.
(30) Chen, Q.; Luo, M.; Wang, T.; Wang, J. X.; Zhou, D.; Han, Y.; Zhang, C. S.; Yan, C. G.; Han, B. H. Porous Organic Polymers Based on Propeller-Like Hexaphenylbenzene Building Units. *Macromolecules* **2011**, *44*, 5573−5577.
(31) Luo, Y.; Li, B.; Wang, W.; Wu, K.; Tan, B. Hypercrosslinked Aromatic Heterocyclic Microporous Polymers: a New Class of Highly Selective CO_2 Capturing Materials. *Adv. Mater.* **2012**, *24*, 5703−5707.
(32) Bhattacharjee, S.; Lugger, J. A. M.; Sijbesma, R. P. Tailoring Pore Size and Chemical Interior of Near 1 nm Sized Pores in a Nanoporous Polymer Based on a Discotic Liquid Crystal. *Macromolecules* **2017**, *50*, 2777−2783.
(33) Liao, Y.; Weber, J.; Mills, B. M.; Ren, Z.; Faul, C. F. J. Highly Efficient and Reversible Iodine Capture in Hexaphenylbenzene-Based Conjugated Microporous Polymers. *Macromolecules* **2016**, *49*, 6322−6333.
(34) Yuan, Y.; Huang, H.; Chen, L.; Chen, Y. N, N′-Bicarbazole: A Versatile Building Block toward the Construction of Conjugated Porous Polymers for CO_2 Capture and Dyes Adsorption. *Macromolecules* **2017**, *50*, 4993−5003.
(35) Fang, Q.; Wang, J.; Gu, S.; Kaspar, R. B.; Zhuang, Z.; Zheng, J.; Guo, H.; Qiu, S.; Yan, Y. 3D Porous Crystalline Polyimide Covalent Organic Frameworks for Drug Delivery. *J. Am. Chem. Soc.* **2015**, *137*, 8352−8355.
(36) Liu, X.; Xu, Y.; Jiang, D. Conjugated Microporous Polymers as Molecular Sensing Devices: Microporous Architecture Enables Rapid Response and Enhances Sensitivity in Fluorescence-On and Fluorescence-Off Sensing. *J. Am. Chem. Soc.* **2012**, *134*, 8738−8741.
(37) Xu, J.; Takai, A.; Bannaron, A.; Nakagawa, T.; Matsuo, Y.; Sugimoto, M.; Matsushita, Y.; Takeuchi, M. A Helically-Twisted Ladder Based on 9,9′-Bifluorenylidene: Synthesis, Characterization, and Carrier-Transport Properties. *Mater. Chem. Front.* **2018**, *2*, 780−784.

https://dx.doi.org/10.1021/acsapm.9b00950
ACS Appl. Polym. Mater. 2020, 2, 528−536

(38) Xu, J. Control over Chiroptical and Electronic Properties of Poly(9,9′-Bifluorenylidene) Bearing Chiral Side Chains. *Polym. Chem.* **2019**, *10*, 6334−6341.
(39) Fichou, D. *Handbook of Oligo- and Polythiophenes*; Wiley-VCH: Weinheim, NY, 1999.
(40) Nakamura, I.; Yamamoto, Y. Transition-Metal-Catalyzed Reactions in Heterocyclic Synthesis. *Chem. Rev.* **2004**, *104*, 2127−2198.
(41) Wang, G.; Morrin, A.; Li, M.; Liu, N.; Luo, X. Nanomaterial-Doped Conducting Polymers for Electrochemical Sensors and Biosensors. *J. Mater. Chem. B* **2018**, *6*, 4173−4190.
(42) Ettinger, A.; Wittmann, T. Fluorescence Live Cell Imaging. *Methods Cell Biol.* **2014**, *123*, 77−94.
(43) Javier, A. E.; Patel, S. N.; Hallinan, D. T.; Srinivasan, V.; Balsara, N. P. Simultaneous Electronic and Ionic Conduction in a Block Copolymer: Application in Lithium Battery Electrodes. *Angew. Chem., Int. Ed.* **2011**, *50*, 9848−9851.
(44) Gerritsen, M.; Kros, A.; Sprakel, V.; Lutterman, J. A.; Nolte, R. J. M.; Jansen, J. A. Biocompatibility Evaluation of Sol-Gel Coatings for Subcutaneously Implantable Glucose Sensors. *Biomaterials* **2000**, *21*, 71−78.
(45) Park, H.; Raffiee, A. H.; John, S. W. M.; Ardekani, A. M.; Lee, H. Towards Smart Self-Clearing Glaucoma Drainage Device. *Microsyst. Nanoeng.* **2018**, *4*, 35−47.
(46) Sun, Y.-B.; Zhao, H.; Mu, D.-L.; Zhang, W.; Cui, J.; Wu, L.; Alam, A.; Wang, D.-X.; Ma, D. Dexmedetomidine Inhibits Astrocyte Pyroptosis and Subsequently Protects the Brain in in Vitro and in Vivo Models of Sepsis. *Cell Death Dis.* **2019**, *10*, 167−180.
(47) Lockhart, J. N.; Spoonmore, T. J.; McCurdy, M. W.; Rogers, B. R.; Guelcher, S. A.; Harth, E. Poly(glycidol) Coating on Ultrahigh Molecular Weight Polyethylene for Reduced Biofilm Growth. *ACS Appl. Mater. Interfaces* **2018**, *10*, 4050−4056.

https://dx.doi.org/10.1021/acsapm.9b00950
ACS Appl. Polym. Mater. 2020, 2, 528−536